Nanostructured Photoactive Films Synthesized by a Flame Aerosol Reactor

Elijah Thimsen and Pratim Biswas
Aerosol and Air Quality Research Laboratory, Dept. of Energy, Environmental and Chemical Engineering, Washington University in St. Louis, St. Louis, MO 63130

DOI 10.1002/aic.11210
Published online June 5, 2007 in Wiley InterScience (www.interscience.wiley.com).

A flame aerosol reactor (FLAR) system was used to deposit nanostructured photocatalytic films of titanium dioxide with well controlled morphologies. Nanoparticles were generated in the aerosol phase and then deposited onto a water-cooled substrate via thermophoresis. Two important parameters that influenced film characteristics were the titanium precursor feed rate and substrate temperature, through their effect on particle sintering dynamics on the substrate. The size of the particles as they arrived at the substrate was controlled by varying the titanium precursor feed rate. When the size was below ~8 nm, sintering was completed in the time available to obtain films with columnar nanostructures. Larger particle sizes resulted in granular, particulate films. The temperature of the substrate was also an important parameter as it controlled the sintering rate and the resultant crystal phase of the film. The thickness of the films was controlled by varying the precursor feed rate and deposition time. The performance of the as-synthesized photocatalytic films was established by measuring the resultant photocurrents. Well sintered columnar morphologies and thicker films (in the range of 40–900 nm) resulted in the largest photocurrents. © 2007 American Institute of Chemical Engineers *AIChE J,* 53: 1727–1735, 2007

Keywords: nanostructured films, titanium dioxide, solar hydrogen, flame aerosol reactor, film synthesis

Introduction

Coatings are applied as films to surfaces for a variety of different applications, such as to form a protective layer to prevent corrosion, to enhance appearance of the base material, for electronics applications, in magnetic media, and in engineered reactors for catalytic applications. The chemical and physical characteristics of the film, such as composition, thickness, and morphology, have to be controlled for specific applications. For example, continuous, nonporous, ceramic films were used to provide corrosion protection to steel surfaces.[1] In contrast, nanoporous, open morphology films were used in photochemical reactors for synthesis of partial-oxygenates by environmentally benign routes.[2] Nanostructured films allow the possibility of obtaining high surface area coatings with tailored characteristics suitable for applications in catalytic reactors.[3]

Titanium dioxide is a wide band-gap semiconducting, ceramic oxide that has been used as a coating material in several different applications for air and water purification, for sulfur removal,[4] for toxic metals capture,[5,6] destruction of bacteria and viruses, self cleaning building materials, and superhydrophillic fog free films.[7] It is the most widely used photocatalyst, because it is relatively safe, inexpensive, and stable to photocorrosion. Another exciting application is the production of hydrogen by a photosplitting reaction of water, which could provide an environmentally benign and sustainable source of hydrogen fuel for the energy industry.[8] Photosplitting of water and many other

Correspondence concerning this article should be addressed to P. Biswas at pratim.biswas@wustl.edu.

solar-energy applications of TiO_2 require that the semiconductor be immobilized as a film. The morphology of the film is an important parameter in establishing the overall effectiveness; for example, a high surface area is desirable if localized chemical reactions are to be promoted, while low internal resistance to mobility of photogenerated charge carriers is also important if these are to be extracted and transported through an external circuit.[8–10] Several studies have identified relationships between film characteristics such as: thickness, morphology and feature size, and the resulting photocatalytic performance.[2,11–14] Film characteristics are primarily determined by the synthesis technique.

There are many synthesis processes used for the deposition of titanium dioxide films. Many of the existing techniques are multi step and require long synthesis times to produce high performance films with desirable morphologies, making them unattractive for industrial scale up. Typical film synthesis processes consist of a deposition step followed by an annealing step. The entire multi step process can take from several hours to a day to complete. Limmer et al.[15] describe a 3–6 h electrophoretic sol–gel process to synthesize TiO_2 nanorods on alumina and polycarbonate substrates for high surface-area applications. For dye sensitized solar cells, dip-coating-annealing processes have been described to synthesize films in 2 h; but the resultant granular films have limited photoactivity due to electron-hole migration barriers at particle–particle interfaces.[16] For photosplitting of water, Varghese et al.[12] describe a 2-step, 17–24 h Ti-foil anodization process to produce TiO_2 nanotubes with controlled thickness; which is used to increase the light to hydrogen conversion efficiency by creating thicker films. To better understand and optimize film performance for important applications like photocatalytic hydrogen production, it is essential to have robust methods to synthesize films with well controlled characteristics.

Flame aerosol reactors (FLAR), which have been an industrially successful route to synthesize nanomaterials, provide a single step process for deposition of nanostructured films.[1] Madler et al.[3] have used FLAR systems for depositing highly porous films relying on thermophoretic deposition. Palgrave and Parkin[17] have described systems using nanoparticle precursors for the synthesis of nanocomposite thin films. Detailed deposition models have also been developed to predict both the film morphology and other characteristics.[18–20] Some studies have demonstrated control over film characteristics through the application of external forces such as electrical fields.[21] However, due to the complex interactions of different process parameters such as precursor concentration, time–temperature history in the flame, deposition rate, time–temperature history on the substrate and many others, there are few studies that relate process conditions to resultant film parameters obtained from single-step FLARs. Specifically, conditions that result in characteristics that are important to photocatalytic applications, such as hydrogen production have not been studied in detail. A more systematic demonstration is essential if practical applications are to be realized.

In this study, a FLAR to deposit nanostructured films of titanium dioxide with controlled morphology and thickness is described. An understanding of the various process parameters, such as precursor feed rate and deposition time, that affect film growth is established. The crystal phase and grain size of the film are established as a function of the process parameters. The resultant photocurrents generated in the films upon exposure to UV irradiation, which is a measure of photoelectric film properties that are important to photocatalytic hydrogen production efficiency, is determined and related to film characteristics.

Experimental Methods

System

The experimental unit consisted of a precursor feed system, a FLAR, and a temperature controlled deposition substrate (Figure 1). The precursor feed system consisted of a bubbler containing titanium isopropoxide (TTIP, Aldrich: 205273, 97% purity) through which argon (Grade 4.8) was bubbled at varying flow rates. The temperature of the bubbler was maintained at 30°C. To prevent condensation of the TTIP, the lines leading up to the flame reactor were heated to ~50°C. The TTIP feed rate was calculated based on the saturation pressure and assumed proportional to the argon flow rate through the bubbler.[22] An additional argon line was added so that the total argon flow rate could be held constant at 2.0 lpm (liters per minute at STP), while varying the flow through the bubbler. The FLAR was a premixed methane–oxygen burner made of a 3/8 "O.D. stainless steel tube with three 1/8" cylinders packed into the middle to achieve an optimal outlet velocity (450 cm/s) through a 0.16 cm^2 area, which prevented flame blow off and extinction. The methane flow rate was fixed at 0.5 lpm (liters per minute at STP) and the oxygen flow rate was fixed at 1.5 lpm, above the stochiometric value of 1.0 lpm for complete combustion. The additional oxygen was provided to ensure complete oxidation of TTIP to produce stoichiometric TiO_2. All gas flow rates were controlled by digital mass flow controllers (MKS Instruments, Wilmington, MA), and the four gas streams were combined and sent through the burner to the flame region (Figure 1).

The flame temperature distribution was measured using a type R thermocouple (Pt-Rh:Pt 2-mm bead) and corrected for radiation from the thermocouple bead. The average flame temperature was 2200 ± 100 K. A temperature controlled substrate was used wherein the titanium dioxide particles formed in the flame were deposited. The substrate used was a square piece of optically polished silicon, 1.5 cm on a side. The silicon substrate was attached to a water-cooled substrate holder to control the temperature of the substrate and the resultant crystal phase of the film (anatase versus rutile). Intimate thermal contact was established between the substrate and heat sink by applying a small amount of silver thermal paste (Arctic Silver, Visalia, CA).

The substrate temperature was controlled by tailoring the thermal resistance of the interface between the substrate and heat sink. If the silicon substrate was pasted directly to the heat sink, the temperature was ~700 K, as measured by a small-bead type K thermocouple cemented to the substrate surface. The thermal resistance of the substrate to heat-sink interface was increased by inserting an intermediate piece of high-temperature glass (Ace-Glass, Vineland, NJ). Under these conditions, the resulting temperature of the substrate was 910 K. An even higher temperature was achieved by inserting a second piece of glass, which increased the sub-

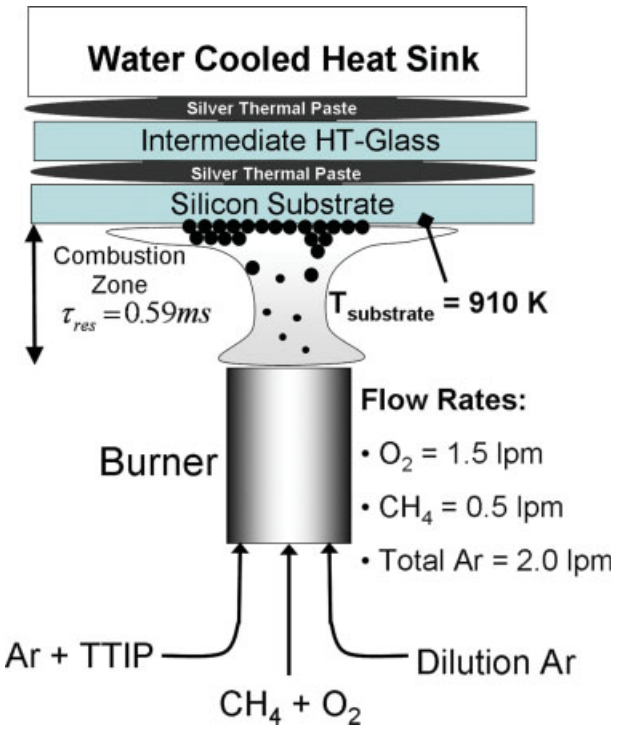

Figure 1. Experimental setup for deposition of nanostructured TiO_2 films.

[Color figure can be viewed in the online issue, which is available at www.interscience.wiley.com.]

strate temperature to ~1080 K. However, unless otherwise stated, only one intermediate piece of glass was used and particles were deposited at a substrate temperature of 910 K. The substrate temperature is important to control, because it alters the morphology of the particle-deposit by altering the sintering rates as discussed in detail in the Results section.

Characterization

Particles in the aerosol phase in the flame region (in the absence of the deposition substrate) were characterized by transmission electron microscopy (TEM) and online scanning mobility particle spectrometry (SMPS) measurements. The particle size distribution was obtained from TEM (JEOL 1200 120 kV) and SMPS (Platform 3080, Nano-DMA 3085, TSI, Shoreview, MN) measurements. It should be noted that the TEM and SMPS measured two different particle size distributions. From TEM images, the primary particle size distribution was obtained, which is the important quantity for dynamic processes such as sintering. The SMPS measured the mobility equivalent aerosol size distribution. The mean size measured by the SMPS could be larger than the primary particle size, especially if agglomeration is prevalent in the system.[23,24]

After deposition, the TiO_2 films where characterized by scanning electron microscopy (SEM) and X-ray diffraction (XRD). The as-produced films were viewed in an SEM (Hitachi model S-4500 field emission electron microscope operating at 15 kV) to determine the film thickness and morphology. For thickness measurements the silicon substrates were cleaved down the middle of the film and attached vertically to the SEM specimen mount. The films were then imaged along a line of sight parallel to the substrate surface to obtain side view images. The crystalline phase and grain size of the films were determined using a Rigaku DMax X-ray diffractometer.

Finally, the photoelectric properties of the films were characterized by photocurrent measurements. The films were deposited onto electrically insulating high-temperature glass substrates (Borosilicate, ACE Glass, Vineland, NJ) at a slightly elevated temperature of 1000 K. Under UV irradiation from a 100 W, 360 nm lamp (Blak–Ray, Model B-100A), the photocurrent was measured by applying a voltage of 22 V to two silver electrodes (SPI supplies, West Chester, PA) that were painted 1 cm apart on the film surface. The current between the electrodes was measured using a picoammeter (Keithly Instruments, Cleveland, OH).

Test plan

Two independent process parameters that affect film characteristics are the TTIP feed rate and deposition time. These parameters were independently varied to determine the effects on the aerosol phase particle size distributions, film grain size, growth rate, film thickness, crystalline phase, and photocurrent. A summary of the experimental parameters and results is presented in Table 1.

Results and Discussion

The gas phase precursor was rapidly oxidized in the high temperature environment to form nanoparticles. These nanoparticles were then directed by thermophoretic forces from the hot gas to the water-cooled substrate and deposited to form a film. There are two important process steps that influence the final film characteristics. The first is formation of TiO_2 particles by oxidation of the TTIP in the high temperature flame environment. The second is restructuring of the particles once they have been deposited onto the substrate via thermophoresis. The influence of these two steps on the final film characteristics is presented in the following sections.

Aerosol phase dynamics

The timescales for different process occurring in the aerosol phase, such as chemical reaction of the precursor and aerosol dynamics, can affect the final film morphology as illustrated in Figure 2. If the characteristic time for the reaction of the TTIP precursor (τ_{rxn}) is larger than the residence time, a chemical vapor deposition (CVD) process would be expected.[25] This would result in TTIP molecules being transported to the substrate and react therein to form the titanium dioxide film. Alternatively, if the characteristic reaction time is less then the residence time, the precursor will react to form particles. Other important time scales in the aerosol phase are the particle–particle characteristic collision time[6] (τ_{coll}) and the particle sintering time[26] (τ_{sin}). Depending on different combinations as illustrated in Figure 2, the deposition process would either be individual particle deposition (IPD) or agglomerated particle deposition (APD).

Table 1. Summary of Experimental Parameters and Results

	Experimental Conditions		Aerosol phase Measurements		Film Measurements				
Exp.	Deposition Time (s)	TTIP Feed Rate (mmol/h)	Fig. 2: Average D_p from TEM (nm)	Fig. 2: Average D_p from SMPS (nm)	Fig. 4: Film Thickness from SEM (nm)	Fig. 4: Crystalline Phase from XRD	Fig. 3: Grain Size From XRD (nm)	Fig. 4: Average Growth Rate (nm/s)	Fig. 6: Photo-Current (nA)
1	90	0.27	–	10.8	180	–	–	2.00	–
2	180	0.069	4.5	4.3	79	Anatase	47.3	0.44	46.86
3	180	0.14	–	7.2	213	Anatase	49.1	1.18	22.10
4	180	0.27	–	10.8	322	Anatase	40.7	1.79	0.64
5	180	0.55	8.0	13.1	2010	Anatase	9.0	11.17	2.53
6	360	0.069	4.5	4.3	233	–	–	0.65	–
7	360	0.27	–	10.8	730	–	–	2.03	–
8	60	0.14	–	7.2	42	Anatase	–	0.70	–
9	90	0.14	–	–	64	Anatase	–	–	2.6
10	120	0.14	–	7.2	86	Anatase	–	0.72	–
11	240	0.14	–	7.2	204	Anatase	–	0.85	–
12	360	0.14	–	–	311	Anatase	–	–	1200
13	480	0.14	–	7.2	417	Anatase	–	0.87	–
14	760	0.14	–	–	692	Anatase	–	–	15,000
15	960	0.14	–	7.2	889	Anatase	–	0.93	–

Constants: methane flow rate = 0.5 lpm; oxygen flow = 1.5 lpm; total argon flow = 2.0 lpm; deposition height = 2 cm above burner; TTIP bubbler temp = 30°C.The column "Photocurrent" corresponds to current measured at 22 V applied voltage.

To determine which deposition process was dominant, the various aerosol phase characteristic times were estimated (Table 2). The residence time in the flame was estimated by assuming that the flame cross-section was equal to the burner outlet area (no jet expansion or ambient fluid entrainment), gases immediately reached the flame temperature and the path-length was equal to the burner-substrate distance of 2 cm. Using these assumptions, a residence time (τ_{res}) of 0.59 ms was calculated. The calculated characteristic reaction time of the TTIP thermal decomposition was 0.12 ms, which was less than the residence time, meaning the TTIP rapidly reacts to form TiO_2 particles in the flame. The characteristic particle–particle collision time assuming 5 nm particles and a TiO_2 molecular concentration calculated from the TTIP feed rate ($\sim 10^{15}$ cm^{-3}) was ~0.1 ms, while the sintering time for the 5 nm particles was 7.4×10^{-5} ms, implying that particles are present as individual spheroids in the flame. Under the flame conditions used in this study, IPD was the dominant process for deposition. Later, the dynamics in the particle-deposit that result in specific morphologies of the film and the relationship of those morphologies to photocurrent generation will be illustrated.

The effect of TTIP feed rate on the particle size distribution is illustrated in Figure 3. The aerosol size distribution was measured online with the SMPS. The primary particle size distribution was measured from TEM images by measuring the diameters of about 130 particles. A log-normal curve fit was performed using Origin (Microcal, v 4.1) to determine distribution parameters. The particle size increased from a mean of 4.5 nm at a TTIP feed rate of 0.069 mmol/h (Test 2) to 8.0 nm at a TTIP feed rate of 0.55 mmol/h (Test 5), as measured by TEM. For the lower TTIP feed rate the SMPS measurement agreed well with the TEM. However, at the higher TTIP feed rate, the SMPS measured a larger diameter than the one obtained from TEM. The discrepancy between the particle size measured from TEM and SMPS at the higher feed rate was likely due to biases that resulted from agglomeration in the dilution probe during sampling. Despite this small discrepancy, the measurements clearly illustrated the trend of increasing particle size with increasing TTIP feed rate.

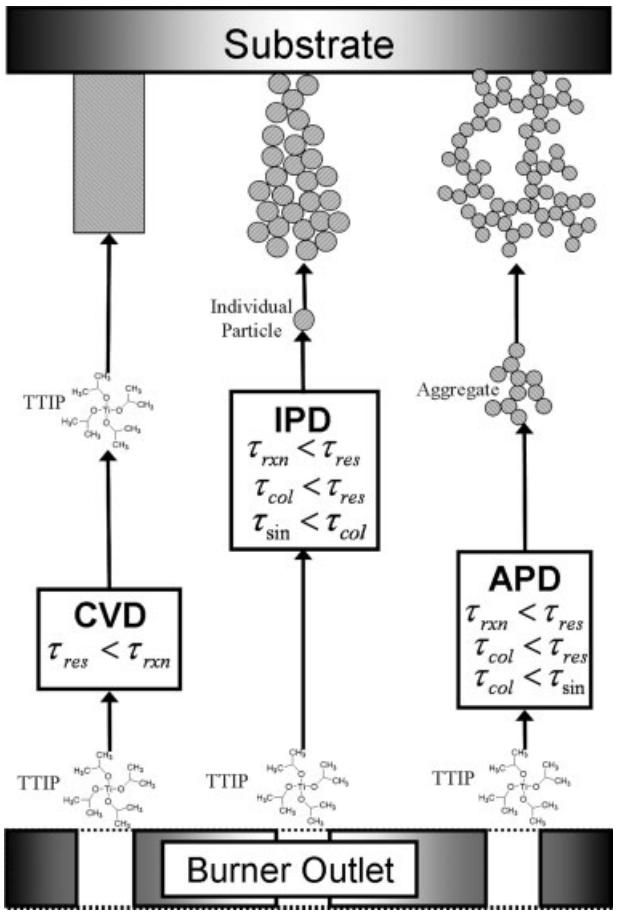

Figure 2. Characteristic time conditions for different film deposition processes: CVD, IPD, and APD.

Table 2. Summary of Estimated Characteristic Times Encountered in the Aerosol Phase

Characteristic Time	Symbol	Value (ms)	Reference
Residence time in flame	τ_{res}	0.59	This work
Thermal decomposition reaction of TTIP to form TiO_2	τ_{rxn}	0.12	Wu and Biswas[6]
5 nm Particle–particle collisions	τ_{col}	~0.1	Wu and Biswas[6]
5 nm Particle sintering at 2200 K	τ_{sin}	7.4×10^{-5}	Kobata et al.[26]

The increase in particle size as a function of TTIP feed rate was due to enhanced coagulational growth in the flame region. At the flame temperature, the reaction to form TiO_2 molecules from TTIP was fast (τ_{rxn} = 0.12 ms, Table 2). Once formed, the TiO_2 molecules collided to form particles, which subsequently grew through a coagulational growth process.[27] The sintering time (τ_{sin}= 7.4×10^{-5} ms, Table 2) was much smaller than the collision time (τ_{coll} ~ 0.1 ms, Table 2) under these conditions, ensuring that near spherical particles resulted from the aerosol phase particle growth process. For a constant residence time, the final size of the coagulational growth process scaled with the initial concentration of TiO_2 molecules, or TTIP feed rate. Through the TTIP feed rate, the size of particles as they arrived at the substrate was tuned to control the restructuring dynamics on the substrate, which is discussed in the following section.

Dynamics after particle deposition onto the substrate

Through its influence on the particle arrival size, which changed the film restructuring dynamics, the TTIP feed rate affected the final film grain size and morphology. The influence of particle arrival size on the film restructuring dynamics can be explained by particle sintering on the substrate. Sintering results in two small particles combining to form a larger structure with a volume equal to the sum of the two initial volumes. At constant temperature, the characteristic time for two TiO_2 particles of the same initial size to completely sinter is proportional to particle diameter to the fourth power.[26,28] From Figure 3, the arrival size of particles at the substrate was ~4.5 and 8.0 nm for TTIP feed rates of 0.069

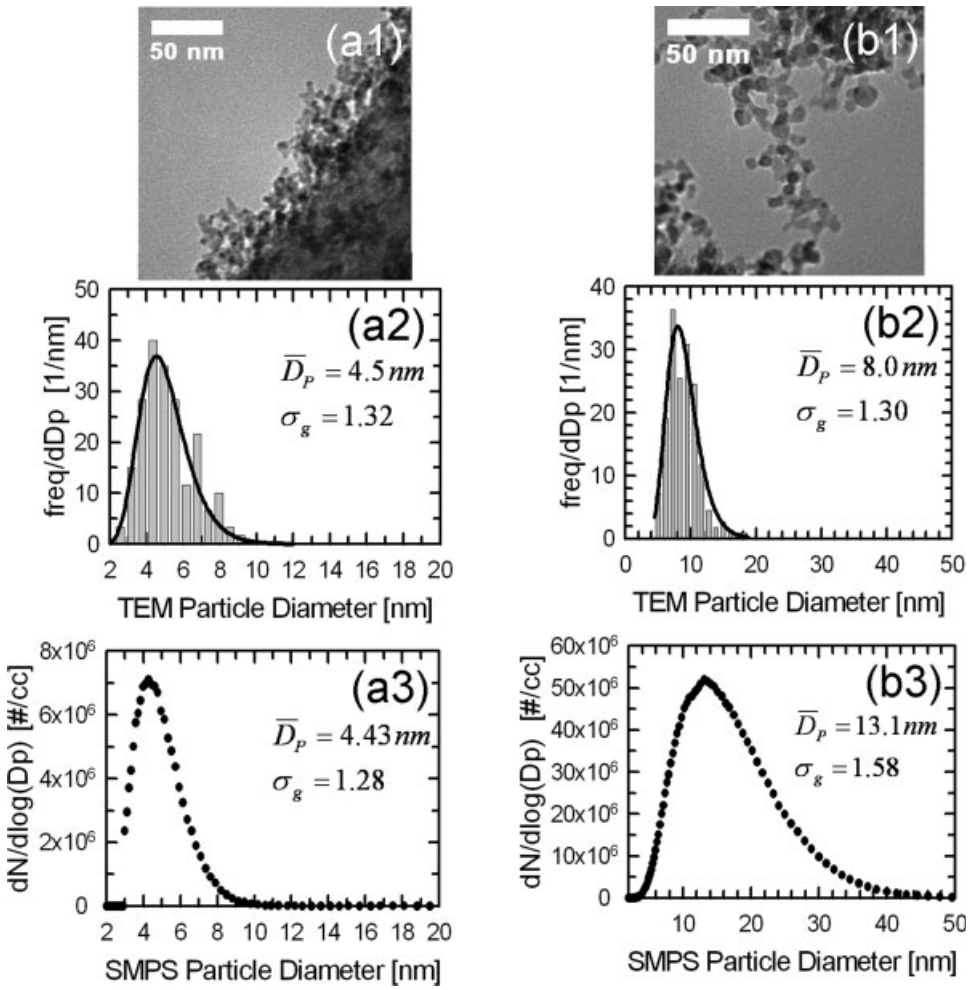

Figure 3. Size measurements of particles in the aerosol phase for two TTIP feed rates.

(a) For TTIP = 0.069 mmol/h: (a1) TEM image of particles; (a2) particle size distribution from TEM images; and (a3) aerosol size distribution measured from the SMPS. (b) For TTIP = 0.55 mmol/h: (b1) TEM image of particles; (b2) particle size distribution from TEM images; and (b3) aerosol size distribution measured from the SMPS.

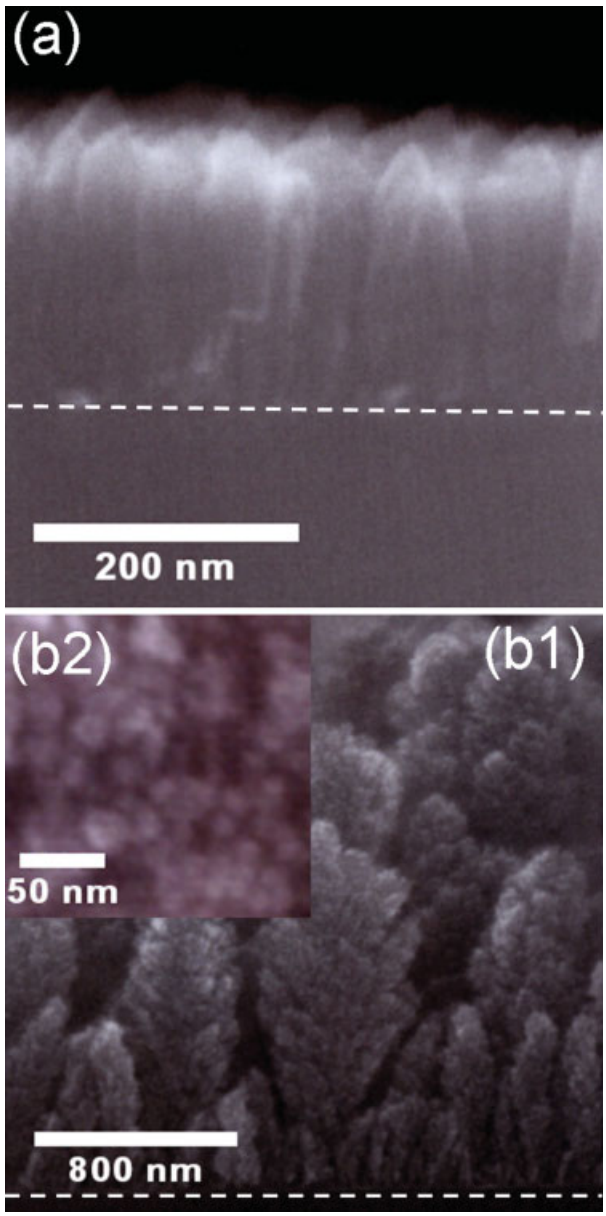

Figure 4. Film morphology for two TTIP feed rate for films deposited for a fixed time of 180 s.

(a) High magnification side view SEM image for TTIP = 0.14 mmol/h. (b) For TTIP = 0.55 mmol/h, (b1) low and (b2) high magnification side view SEM images. [Color figure can be viewed in the online issue, which is available at www.interscience.wiley.com.]

mmol/h (Test 2) and 0.55 mmol/h (Test 5), respectively. The characteristic sintering time for the higher TTIP feed rate was an order of magnitude longer than for the lower TTIP feed rate, thus changing the sintering dynamics and final film morphology. This difference in morphology can be seen in Figure 4.

For small particle arrival size, or fast sintering dynamics, a columnar structure was observed. The sintered columnar morphology was characterized by continuous vertical columns, observed in the SEM, and large average grain size, measured from XRD peak broadening using the Scherrer equation. As small particles, which were 4.5 nm in the aerosol phase, sintered, they combined to form larger structures that had longer range crystalline order, hence the 47 nm grain size observed in the XRD (Test 2).

Alternatively, for large particle arrival size, or slow sintering dynamics, a granular particulate morphology was observed. The particulate morphology was characterized by fractal structures, observed in the SEM and a small average grain size. Because of the slow sintering dynamics, the large particles did not combine and instead remained isolated with approximately the same grain size as was present in the original particle before it deposited. This can be seen by comparing the average grain size of the unsintered film deposited at 0.55 mmol/h TTIP feed rate (Figure 5) to the aerosol phase particle size from TEM at the same conditions (Figure 3). Because of the 2200 K flame temperature, the particles in the aerosol phase were expected to be nearly single crystal. From the TEM measurements, the large particles were ~8 nm before they deposited onto the substrate, which is similar to the 9 nm grain size of the film, which would be expected if the particles did not experience significant sintering once deposited onto the substrate.

The temperature of the substrate (film) also affects the sintering rate.[26,28] Temperature could also be used as a process parameter to control the morphology of the film. This was verified qualitatively by changing the substrate to heat sink thermal resistance, to alter the substrate temperature. At low temperatures, particulate films were observed in the SEM, due to low rates of sintering amongst the deposited particles. At higher substrate temperatures, well sintered columnar films were obtained that were similar in appearance to the sintered columnar SEM images (Figure 4a). However, if one increases the temperature further, the films will anneal out and the columnar structures are expected to collapse as predicted by the models developed by Kulkarni and Biswas.[20] Furthermore, undesirable crystal phase transitions from anatase to rutile will take place at elevated temperatures, which

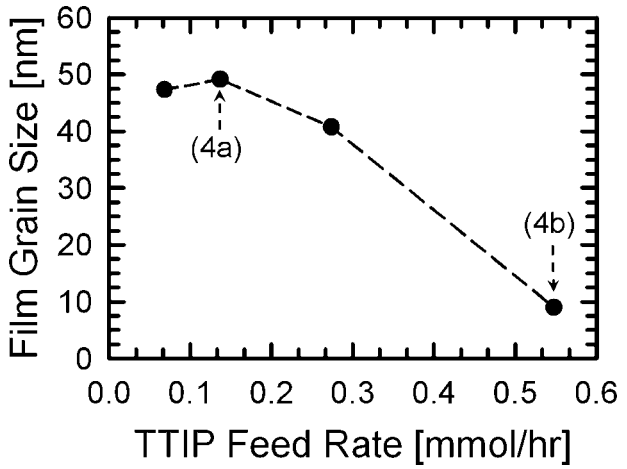

Figure 5. Average grain size measured from XRD peak broadening as a function of TTIP feed rate, for a fixed deposition time of 180 s.

The points labeled as 4a and 4b correspond to the same films as the SEM images in Figure 4.

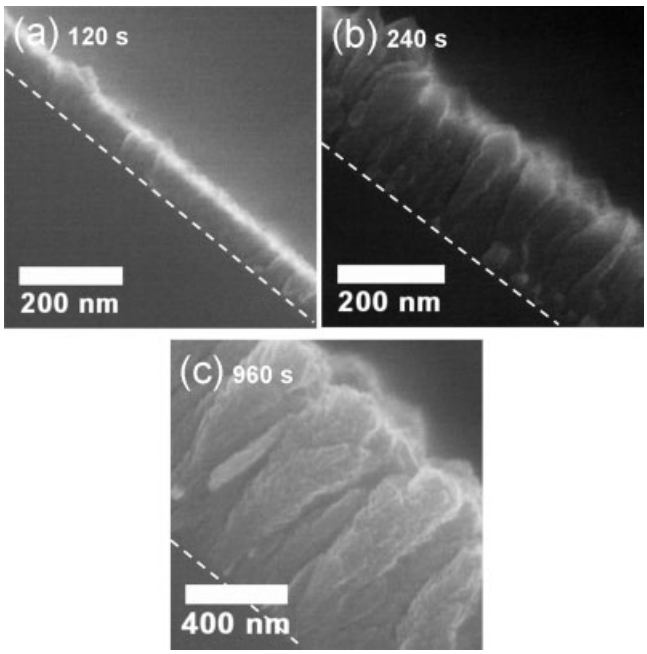

Figure 6. Selected side view SEM images of films showing film thickness increasing with deposition time for a fixed TTIP feed rate of 0.14 mmol/h: (a) 120 s, (b) 240 s and (c) 960 s.

[Color figure can be viewed in the online issue, which is available at www.interscience.wiley.com.]

precludes increasing the substrate temperature substantially beyond 600°C.

The film thickness can be controlled by both the deposition time and TTIP feed rate. Films were deposited for different times and imaged by SEM to measure thickness. In Figure 6, selected side view SEM images are shown that illustrate the evolution of film thickness for several deposition times. For the times tested, the film thickness increased roughly linearly with deposition time (Figure 7). In addition, the growth rate increased with TTIP feed rate, which was reasonable considering the increased mass flux to the substrate.

Photocurrent measurements

With precise control over both the film morphology and thickness, photocurrent measurements were performed to understand the relationship between film characteristics and photoactivity. A simple electrical circuit was created by connecting lead wires to the film and a DC power supply. A voltage of 22 V was applied and the resulting current was measured using a picoammeter. Photocurrent measurements were taken for films deposited at several TTIP feed rates and deposition times (Figure 8). The photocurrent was at the noise level of the picoammeter when the UV lamp was switched off.

Morphology had a significant effect on the photocurrent. The films deposited at lower TTIP feed rates exhibited greater photocurrents than the films formed with higher TTIP feed rates. At lower TTIP feed rates, the films had a sintered columnar like structure with a large grain size. At higher TTIP feed rates, the films had a particulate like structure with a small average grain size. The photocurrent is related grain size, but also depends on interfacial properties and can change for slight alterations of the film morphology. For instance, it is more difficult for free charge carriers to migrate to the electrodes in particulate films with small grain size because of particle–particle interfacial migration barriers.[16] In continuous and well sintered films with larger grain size, free charge carriers encounter fewer migration barriers and can freely flow to the electrodes. This result is in agreement with other work that has found higher electron drift mobility in columnar films, compared with granular particulate films.[29]

The photocurrent was larger for the thicker films (longer deposition times), while maintaining the well sintered, columnar morphology. As the thickness of the sintered columnar film was increased, it intercepted more light, thus generating an increased number of free charge carriers. The increased number of free charge carriers resulted in an increase in the measured photocurrent. It should be noted that there may be an upper limit on thickness beyond, which the photocurrent could saturate due to no further increase in light absorption (due to geometrical effects). These photocurrent measurements illustrate that the deposited films are photoactive and there are clear trends in the photoactivity as a function of controllable film characteristics.

Conclusions

A robust system consisting of a FLAR for the deposition of TiO_2 films has been developed. The ability to synthesize films with well controlled morphology in a single-step process was described. Two important process parameters that influence the film morphology are TTIP feed rate and the substrate temperature. These parameters influence the final film morphology through their effect on particle sintering dynamics on the substrate. The range of particle arrival sizes was varied from 4.5 to 8.0 nm. Smaller particle arrival sizes ensure faster sintering after deposition resulting in the formation of well sintered, columnar morphology films. For larger

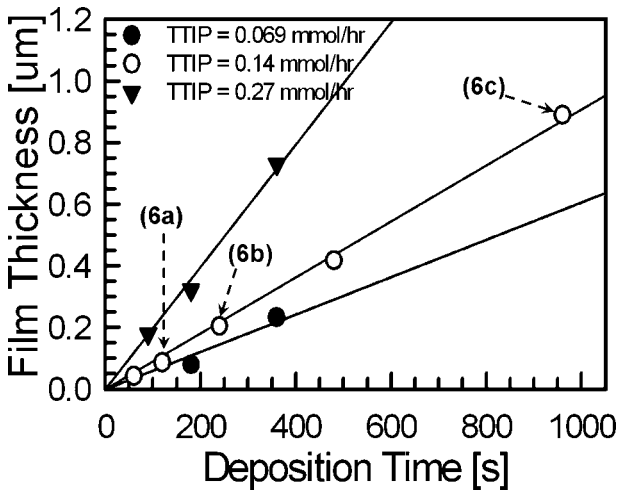

Figure 7. Film thickness plotted as a function of deposition time for 3 different TTIP feed rates.

The points labeled as 6a, 6b, and 6c correspond to the SEM images in Figure 6.

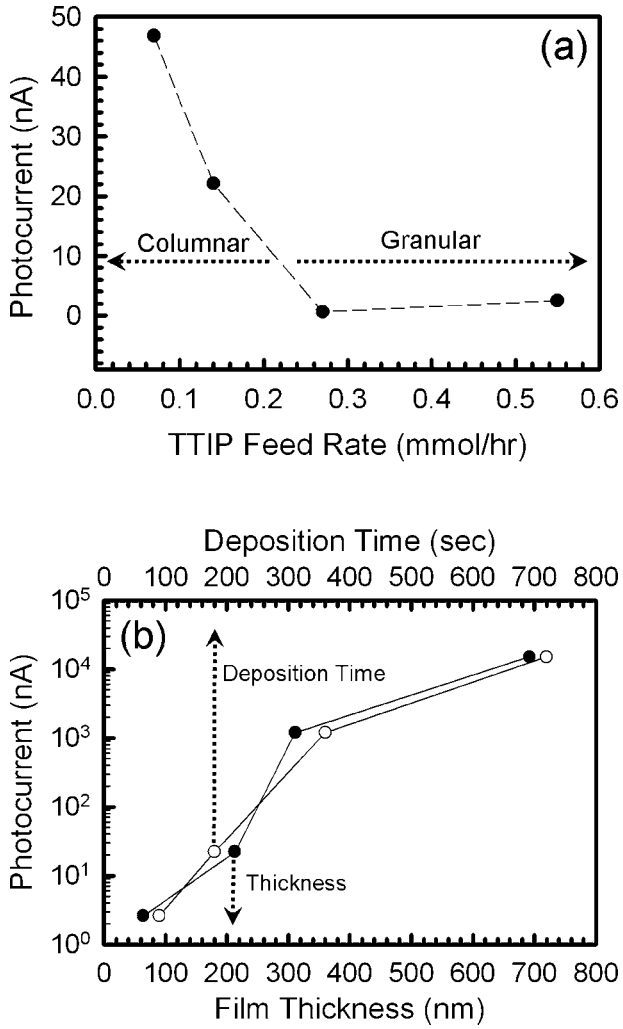

Figure 8. Measured photocurrents as a function of: (a) TTIP feed rate for a fixed deposition time of 180 s. and (b) deposition time (film thickness) for a fixed TTIP feed rate of 0.14 mmol/hr.

particle sizes, the sintering on the substrate is much slower, leading to a granular morphology. Good control of the film thickness was demonstrated, and the relationship to deposition time and precursor feed rate established.

The titanium dioxide films were demonstrated to be activated by light. The resultant photocurrents were measured and the performance of the well sintered, columnar morphology films was found to be superior to the granular films. Similarly, thicker films in the range of 42–890 nm were demonstrated to have higher photocurrents. These photocurrent results are a measure of the photoelectric properties of the films, which are likely critical to applications such as photocatalytic hydrogen production by watersplitting. Work is currently underway to apply these films to photocatalytic watersplitting.

The FLAR could likely be scaled up and applied to the deposition of many metal-oxide films for which suitable precursors are available. Fe_2O_3 films have been synthesized by switching the precursor in the bubbler from TTIP to $Fe(CO)_5$, and is the subject of a future study.

This study provides insights into design parameters and operating conditions necessary to obtain desired film morphologies. For example, if well sintered columnar films are desired, the particle arrival size and the substrate temperature would have to be within a certain range. The particle arrival size is controlled by the flame operating conditions and feed rate of the precursor. The results indicate that beyond a certain feed rate, the resultant particle size would be large so that well sintered columnar morphologies would not be obtained.

Acknowledgments

We acknowledge partial support from the Center for Environmentally Beneficial Catalysis (CEBC) National Science Foundation Engineering Research Center Grant (ERC-0310689), the NSF-NIRT 0304649 Grant, and the Center for Materials Innovation (CMI) at Washington University in Saint Louis.

Literature Cited

1. Yang G, Biswas P, Boolchand P, Sabata A. Deposition of multifunctional titania films by aerosol routes. *J Am Ceram Soc*. 1999;82:2573–2579.
2. Sahle-Demessie E, Gonzalez M, Wang MZ, Biswas P. Synthesizing alcohols and ketones by photoinduced catalytic partial oxidation of hydrocarbons in titania film reactors prepared by three different methods. *Ind Eng Chem Res*. 1999;38:3276–3284.
3. Madler AL, Roessler A, Pratsinis SE. Direct formation of highly porous gas-sensing films by in-situ thermophoretic deposition of flame-made Pt/SnO_2 nanoparticles. *Sens Actuators B*. 2006;114:283–295.
4. Beck DD, Siegel RW. The dissociative adsorption of hydrogen-sulfide over nanophase titanium-dioxide. *J Mater Res*. 1992;7:2840–2845.
5. Wu CY, Lee TG, Tyree G, Arar E, Biswas P. Capture of mercury in combustion systems by in situ-generated titania particles with UV irradiation. *Environ Eng Sci*. 1998;15:137–148.
6. Biswas P, Wu CY. Control of toxic metal emissions from combustors using sorbents: a review. *J Air Waste Manage Assoc*. 1998;48:113–127.
7. Fujishima A, Hashimoto K, Watanabe T. TiO_2 Photocatalysis, Fundamentals and Applications, 1st ed. Japan: BKC, 1999.
8. Herrmann JM. Heterogeneous photocatalysis: state of the art and present applications. *Top Catal*. 2005;34:49–65.
9. Gratzel M. Photoelectrochemical cells. *Nature*. 2001;414:338–344.
10. Nanu M, Schoonman J, Goossens A. Nanocomposite three-dimensional solar cells obtained by chemical spray deposition. *Nano Lett*. 2005;5:1716–1719.
11. Adachi M, Murata Y, Okada I, Yoshikawa S. Formation of titania nanotubes and applications for dye sensitized solar cells. *J Electrochem Soc*. 2003;150:G488–G493.
12. Varghese O, Paulose M, Shankar K, Mor G, Grimes C. Water-photolysis properties of micron-length highly-ordered titania nanotube-arrays. *J Nanosci Nanotechnol*. 2005;5:1158–1165.
13. Gratzel M. Solar energy conversion by dye-sensitized photovoltaic cells. *Inorg Chem*. 2005;55:6841–6851.
14. O'Hayre R, Nanu M, Schoonman J, Goossens A, Wang Q, Gratzel M. The influence of TiO_2 particle size in TiO_2/CuInS nanocomposite solar cells. *Adv Funct Mater*. 2006;16:1566–1576.
15. Limmer SJ, Chou TP, Cao CZ. A study on the growth of TiO_2 nanorods using sol electrophoresis. *J Mater Sci*. 2004;39:895–901.
16. Jongh PE, Vanmaekelbergh D. Trap-limited electronic transport in assemblies of nanometer-sized TiO_2 particles. *Phys Rev Lett*. 1996;77:3427–3430.
17. Palgrave RG, Parkin IP. Aerosol assisted chemical vapor deposition using nanoparticle precursors: a route to nanocomposite thin films. *J Am Chem Soc*. 2006;128:1587–1597.
18. Madler L, Lall A, Friedlander S. One-step aerosol synthesis of nanoparticle agglomerate films: simulation of film porosity and thickness. *Nanotechnology*. 2006;17:4783–4795.

19. Kulkarni P, Biswas P. A Brownian dynamics simulation to predict morphology of nanoparticle deposits in the presence of interparticle interactions. *Aerosol Sci Technol*. 2004;38:541–554.
20. Kulkarni P, Biswas P. Morphology of nanostructured films for environmental applications: simulation of simultaneous sintering and growth. *J Nanopart Res*. 2003;5:259–268.
21. Krinke TJ, Fissan H, Deppert K. Deposition of aerosol nanoparticles on flat substrate surfaces. *Phase Transitions*. 2003;76:333–345.
22. Okuyama K, Kousaka Y, Tohge N, Yamamoto S, Wu JJ, Flagen RC, Seinfeld JH. Production of ultrafine metal oxide aerosol particles by thermal decomposition of metal alkoxide vapors. *AIChE J*. 1986;32:2010–2019.
23. Namiki N, Cho K, Fraundorf P, Biswas P. Tubular reactor synthesis of doped nanostructured titanium dioxide and its enhanced activation by coronas and soft X-rays. *Ind Eng Chem Res*. 2005;44:5213–5220.
24. Nakaso K, Fujimoto T, Seto T, Shimada M, Okuyama K, Lunden MM. Size distribution change of titania nano-particle agglomerates generated by gas phase reaction, agglomeration, and sintering. *Aerosol Sci Technol*. 2001;35:929–947.
25. Chen CH, Schoonman J. Thin-film techniques for advanced energy conversion and storage systems. *J Ind Eng Chem*. 2004;10:1114–1125.
26. Kobata A, Kusakabe K, Morooka S. Growth and transformation of TiO_2 crystallites in aerosol reactor. *AIChE J*. 1991;37:347–359.
27. Friedlander S. Smoke Dust and Haze: Fundamentals of Aerosol Dynamics, 2nd ed. New York: Oxford University Press, 2000.
28. Cho K, Biswas P. Sintering rates for pristine and doped titanium dioxide determined using a tandem differential mobility analyzer system. *Aerosol Sci Technol*. 2006;40:309–319.
29. Aduda BO, Ravirajan P, Choy KL, Nelson J. Effect of morphology on electron drift mobility in porous TiO_2. *Int J Photoenergy*. 2004;6:141–147.

Manuscript received Jan. 29, 2007, and revision received Apr. 7, 2007.